



# Triazolone/alginate-zinc (II)-montmorillonite sustained release system with improved adsorption capacity and pH-sensitivity

Huayao Chen<sup>1,2</sup> · Jinghui Zhan<sup>1</sup> · Hongjun Zhou<sup>1,2</sup> · Li Hao<sup>1,2</sup> · Hua Xu<sup>1,2</sup> · Xia Pu<sup>1,2</sup> · Xinhua Zhou<sup>1,2</sup>

Received: 16 September 2020 / Accepted: 16 November 2020 / Published online: 22 November 2020  
© Springer Nature Switzerland AG 2020

## Abstract

Developing effective sustained release system is an efficient way to prevent the pollution from overused pesticide. Hence, a highly efficient sustained release system was developed using zinc (II) modified montmorillonite (Zn-Mt) prepared by ion exchange from sodium montmorillonite (Na-Mt) with zinc nitrate. Zn-Mt was modified by sodium alginate (ALG) to further improve its sustained release performance and pH-sensitivity. The results indicated that triazolone was supported on the zinc modified montmorillonite through the coordination bond from zinc ion. The zinc ion in the Mt also played a similar role as calcium ion to induce ALG crosslinking which made ALG highly dispersed in the pores of Mt. ALG interacted with  $Zn^{2+}$  from Mt through electrostatic interaction and wined with triazolone to form a barrier for the sustained release system. As a result, the adsorption capacity of ALG-Zn-Mt (17.75 mg/g) was improved comparing with Na-Mt without modification (14.52 mg/g). The sustained release performance of ALG-Zn-Mt showed also significant pH-sensitivity in accordance with the stability of ALG.

**Keywords** Montmorillonite, · Zinc (II), · Alginate, · Sustained release

## 1 Introduction

Nowadays, researchers and industries are in constant quest of designing cost-effective, multipurpose, and robust nanocomposite system for advanced material applications [1–3]. Among them, nanoparticles containing pesticides showed an excellent performance against pests due to its high BET surface, high bioactivity and sustained release performance. Moreover, the dose of pesticide used is very less in nanoformulation and, hence minimizes potential negative effect associated with overdose. However, reports on controlled release of pesticide nanoformulations are far less than reports of applications in human medicine reported.

Recently, Kumar et al. [4] adopted alginate (ALG)- biodegradable, biocompatible, and natural marine-based

polysaccharides which are linear copolymers with a block-wise pattern along the linear chain [5] and applied widely in drug delivery [6–9] to synthesis pesticide (imidacloprid) loaded sodium alginate nanoparticles. Alginate encapsulated nanoformulation presented more effective than plane pesticide. The toxicity analysis of dummy, loaded, and plane formulations were also carried out. Furthermore, the negatively charged carboxylate acid groups from alginate can interact with the positively charged groups by ionic bonds to create pH sensitive complexes [10]. In our previous work, mesoporous silica was modified with ALG to increase the steric hindrance which presented satisfying sustained release performance [9] comparing with pure mesoporous silica carrier [11]. However, the expensive price and complex preparation process of mesoporous silica prevents its practical application. Meanwhile,

✉ Huayao Chen, huayao\_011@163.com; ✉ Xinhua Zhou, cexinhuazhou@163.com | <sup>1</sup>School of Chemistry and Chemical Engineering, Zhongkai University of Agriculture and Engineering, Guangzhou, China. <sup>2</sup>Key Laboratory of Agricultural Green Fine Chemicals of Guangdong Higher Education Institution, Guangzhou, China.



environment-friendly Mt with low cost and high surface activity should be more attractive in pesticide sustained release formulations. Montmorillonite (Mt) with a layered silicate of 2:1 type was one of the most widely used adsorbent ordered layered pores due to its high porosity, low cost, and high capacity [12, 13]. In addition, its natural two-dimensional (2D) nanosheet-shaped layered structure also has high specific surface area, abundant active sites [14]. Therefore, Mt was widely applied in toxic organic pollutants removal and industrial wastes remediation [15, 16]. The preparation of montmorillonite-alginate has been reported in literature which used as drug delivery carriers and adsorbents [5, 17, 18]. For example, Jain et al. [5] adopted montmorillonite (Mt) to prepare Mt-based alginate beads as a delivery vehicle for oral administration of drugs which can effectively reduce the multiple dosing frequency. Besides, the prepared sustained release system usually showed pH-sensitivity as the universal characteristic of clay minerals [19] which was beneficial to the pest control in agriculture [20–22]. And the addition of montmorillonite to formulation was found to have a profound inhibitory effect on the release of pesticide reported by previous research [23]. However, the negative charge montmorillonite decreased the strength of interaction with the negatively charged carboxylate acid groups from alginate.

In order to obtain a highly efficient pesticide sustained release system and a deeper understanding of the pesticide release process in the prepared carrier, Mt modified with zinc ion which was expected to decrease its negative charge was encapsulated with ALG to further improve its sustained release performance. Triazolone- an efficient fungicide which also presented huge potential in weed control [24] was adopted as a model pesticide. Because triazolone molecule has three nitrogen atoms providing lone pair electrons for coordination. The interactions among ALG, zinc ion, and montmorillonite as well as the release kinetic behavior were investigated to reveal the pesticide sustained release mechanism. Furthermore, the sustained release tests under different pH conditions were also performed to evaluate the pH-sensitivity of the samples.

## 2 Experimental

### 2.1 Chemical reagents

Ethanol, zinc nitrate, hydrochloric acid solution, sodium hydroxide, sodium bicarbonate, hydrochloride, and cetyl trimethyl ammonium bromide (CTAB) were purchased from Damao Chemical Reagents (Tianjin, China). Montmorillonite K-10 clay (Mt) and sodium alginate (ALG) were obtained from Aladdin (Shanghai, China). Triazolone form

Jiangsu Jinghong Chemical Engineering Co., Ltd. (Jiangsu, China) was also adopted in this work. In addition, sodium montmorillonite clay (Na-Mt) was prepared through Mt modified by sodium bicarbonate at proportion of 6% at 80 °C for 6 h. All of the chemical reagents used in the experiments were of analytical grade. The water was double deionized water.

### 2.2 Preparation of Zn-Mt

100 mL of zinc nitrate solution with different concentration (0.5 mol/L) was added to 1 g of Na-Mt at 35 °C under stirring for 24 h. Then Zn-Mt was attained after being filtered, washed, and dried. In order to improve its organic adsorption capacity, Zn-Mt and Na-Mt were immersed in CTAB solution (15 mg/mL) at 80 °C for 10 h under stirring before encapsulated by ALG and used for characterization or supporting triazolone.

### 2.3 ALG encapsulation

The sample prepared (100 mg) was added into 20 mL deionized water under stirring, then mixed with 10 mL ALG solution (5.5 mg/mL) through injection dropwisely. Then the samples were filtered, washed and dried to obtain the products after string for 4 h which were denoted as ALG-Na-Mt and ALG-Zn-Mt according to different samples.

### 2.4 The loading of pesticide

Triazolone was supported via impregnation method. The samples were under vacuum treatment at 80 °C for 6 h. And then 0.05 g sample was added in 25 mL of triazolone ethanol solution (0.5 mg/mL) at 35 °C, and the mixture was stirred for 24 h. before centrifuged and dried. The products obtained were denoted as Tri/Na-Mt, Tri/Zn-Mt, Tri/ALG-Na-Mt, and Tri/ALG-Zn-Mt, respectively. And the filter liquor was characterized by UV-2550 UV-Vis spectrophotometer from Shimadzu Co., Japan to calculate the adsorption capacity by the following equation:

$$AC = \left( \frac{C_0 - C_1}{m} \right) \times V \quad (1)$$

In Eq. 1, the mass concentration (mg/L) of the triazolone in ethanol solution before and after adsorption was represented by  $C_0$  and  $C_1$ , respectively;  $m$  was the mass (g) of samples. Before measurement, the relationship between the solution concentration ( $C$ /(mg\*L<sup>-1</sup>)) and absorbance ( $A$ ) was fitted with linear regression through different concentrations at  $\lambda = 223$  nm to obtain the equation:  $A = 0.0391C - 0.1079$ ,  $R^{2h} = 0.996$ .

## 2.5 Sustained release performance

The sustained release of the samples was performed according to the reference [10]. The carriers were weighed as  $M_1$  (mg) and put into three flask with 50 mL of 50% ethanol. At intervals of (t), 3 mL of the sample solution was withdrawn. The cumulative release amount of triazolone was calculated as  $R_i$  at time t according to the standard curvilinear equation:  $A = 0.0364C + 0.0153$ ,  $R^2 = 0.999$  before added back to the conical flask, and three replicates were prepared and kept under standard. Furthermore, the  $R_i$ -t curve was drawn to fit different release kinetic equations.

## 2.6 Characterization techniques

The FTIR spectra were recorded by Spectrum 100 Fourier infrared spectrometer (PerkinElmer Inc., USA). The samples were diluted in solid KBr before the spectrum recording. An S4800 scanning electron microscope (Hitachi, Japan) was used to observe the surface topography which the samples were gold sputtered before SEM analysis. Bruker AXS D8 X-ray diffractometer (Karlsruhe, Germany) with Cu radiation ( $\lambda = 1.5418 \text{ \AA}$ ) and a graphite monochromator at 25 °C, 40 kV, and 30 mA were adopted to perform XRD analysis in the range of  $2\theta$  from 5° to 90° at 10°/min in 0.02°2 $\theta$  step size for wide angle XRD and at 2°/min (angular range  $2\theta = 0.5 \sim 10^\circ$ ) in 0.02°2 $\theta$  step size for small angle XRD.  $N_2$  adsorption isotherms at 77 K were operated on Quadrasorb SI adsorption equipment (Quantachrome, USA) before degassed at 200 °C for 12 h in vacuum. Thermogravimetric analyses were performed by Q200 differential scanning calorimeter (TA Co., USA) to conduct differential scanning calorimetry (DSC). X-ray photoelectron spectra (XPS, Thermo Fisher Scientific, USA) equipped with a monochromatic Al K $\alpha$  X-ray source ( $h\nu = 1,486.6 \text{ eV}$ ) was used to study the valence state and elemental quantification of samples. The zeta potential of the sample suspension was measured by the Zetasizer Nano ZS (Malvern Instruments, UK) in deionized water under neutral condition through ultrasonic dispersion before measurement. And three replicates were prepared and kept under standard. While hydrochloric acid solution and sodium hydroxide were adopted to change the solution pH as in the sustained release performance.

## 3 Results and discussion

### 3.1 Structure characterization

FTIR was performed to study the different composition of the samples as depicted (Fig. 1). The peaks centered at

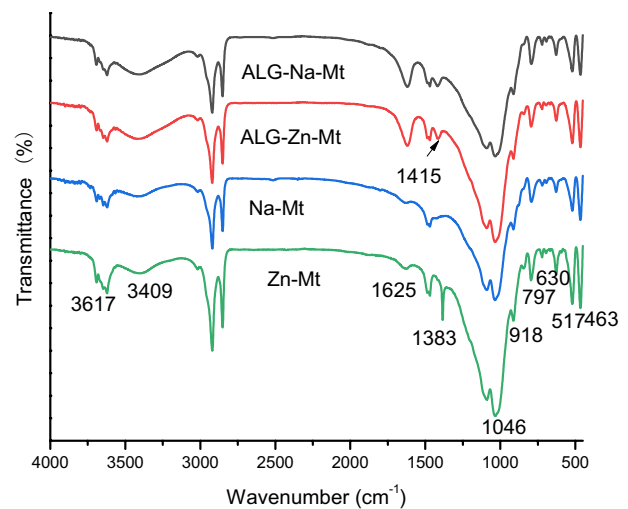
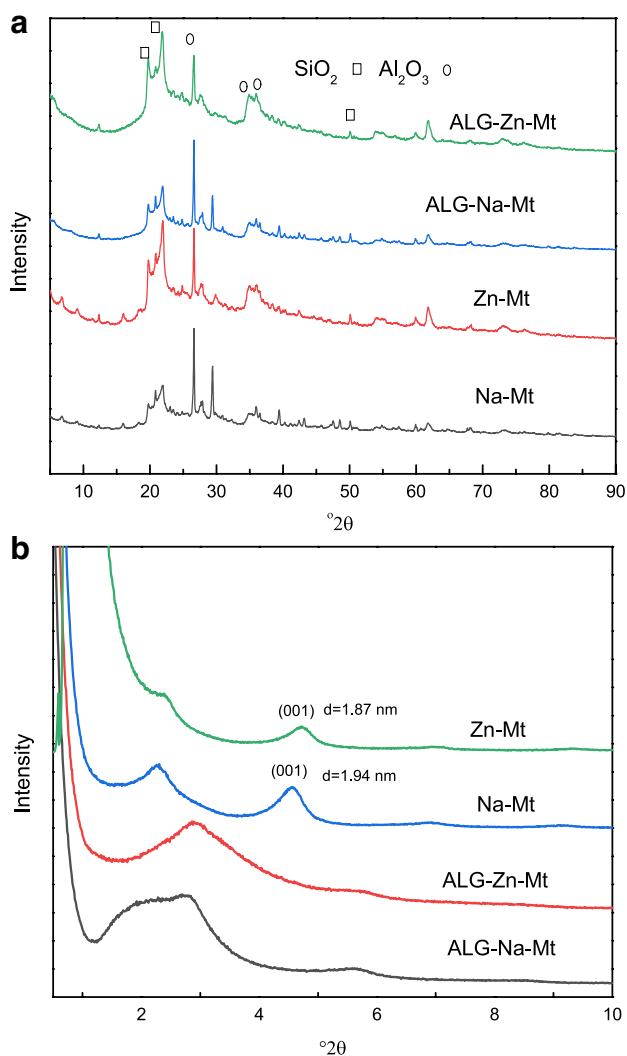


Fig. 1 FTIR spectra of Na-Mt, Zn-Mt, ALG-Na-Mt, and ALG-Zn-Mt

3409  $\text{cm}^{-1}$ , and 3617  $\text{cm}^{-1}$  corresponded to OH stretching mode in molecular water and in Si-OH, Al-OH bonds, respectively; The peaks at 1042  $\text{cm}^{-1}$ , 630  $\text{cm}^{-1}$ , and 517  $\text{cm}^{-1}$  were ascribed to stretching vibration of the Si-O bonds, stretching vibration of Si-O-Al bonds and the bending vibration of Si-O-Al bonds [18]; bands at 918  $\text{cm}^{-1}$  and 797  $\text{cm}^{-1}$  were corresponded to Al-Al-OH bending, and Si-O bending in Mt; the peak of 463  $\text{cm}^{-1}$  belonged to Si-O-Si and Na-Al-OH vibration. Nitrate ions from  $\text{Zn}(\text{NO}_3)_2$  salt appeared at 1383  $\text{cm}^{-1}$ . Sodium alginate presented asymmetric and symmetric stretching vibrations of carboxyl anions at 1625  $\text{cm}^{-1}$  and 1415  $\text{cm}^{-1}$ ; -OH stretching vibration at 3409  $\text{cm}^{-1}$  [17]. And the bands of 1625  $\text{cm}^{-1}$  and 3409  $\text{cm}^{-1}$  ascribed to  $\text{COO}^-$  group and OH group from ALG were remarkably enhanced for ALG-Zn-Mt and ALG-Na-Mt.

The XRD patterns of Na-Mt, Zn-Mt, ALG-Na-Mt, and ALG-Zn-Mt (Fig. 2a) were presented to show the characteristic peaks of Mt in which the main mineralogical composition  $\text{SiO}_2$  and  $\text{Al}_2\text{O}_3$  of the samples was marked above the pattern. However, the broadening of reflections after zinc modification indicated the randomness in the interlayer of the lattice brought by the Jahn-Teller distorted  $\text{Zn}^{2+}$ -ions. The d-spacing of the Na-Mt and Zn-Mt were 1.87 nm and 1.94 nm calculated from characteristic peak shown in small angle XRD spectrum in Fig. 2b ascribed to (001) crystal face characterized as a layered structure and corresponded to the basal spacing, respectively. Comparing the XRD spectrum of before and after zinc modification, a decrease in the d-spacing was observed after zinc modification confirming that the zinc ion was intercalated into layer structure of Mt. The completely loss of d (001) peaks were observed for ALG-Na-Mt and ALG-Zn-Mt which is a clear indication of the enlargement of the basal



**Fig. 2** Wide angle XRD patterns (a) and small angle XRD patterns (b) of Na-Mt, Zn-Mt, ALG-Na-Mt, and ALG-Zn-Mt

spacing of the clay as a result of the interactions between Mt and alginate in accordance with previous report [18].

As shown by the DSC curves in Fig. 3, the endothermic peak of adsorbed water from zinc modified Mt shifted from 148 °C to 133 °C due to the  $\text{Zn}^{2+}$  intercalation. However, the fusion peak of triazolone at 80 °C disappeared after being loaded into vehicles suggesting that triazolone was distributed in the amorphous state on vehicles. Similarly, the fusion peak of ALG at 135 °C also disappeared after encapsulated on Mt indicating that ALG was also in amorphous state due to the confinement effect of the layer structure from Mt.

As shown by the SEM images (Fig. 4a), the surface of pure Na-Mt with layer structure was smooth. The surface became rough after zinc modification (Fig. 4b). After encapsulated by ALG (Fig. 4c) for, a ropy thin layer was detected on the surface of ALG-Na-Mt. And the some

pores were blocked by this ropy layer. The obtained ALG-Zn-Mt SEM images shown in Fig. 4d indicated that the encapsulation of Zn-Mt by ALG was performed more favorably than Na-Mt with a thicker ropy layer. However, its pore-blocked phenomenon was not as significant as ALG-Na-Mt because the zinc induced the cross-linking of alginate evenly to prevent ALG agglomeration in pores. In additional, a porous and rough structure appeared evidently for ALG-Zn-Mt which was an appropriate characteristic for efficient adsorption [18].

Zeta potential studies of Na-Mt, Zn-Mt, ALG-Na-Mt, and ALG-Zn-Mt (Table 1) were investigated at pH=7 based on PALS phase light scattering technique (PALS) method. The Zeta potential of Na-Mt shifted from -24.66 mV to 16.29 mV after modified by zinc ion owing to the positive charge from zinc ion. After ALG encapsulation, the Zeta potential of Na-Mt and Zn-Mt decreased from -24.66 mV and 16.29 mV to -28.98 mV and -19.65 mV, respectively, caused by the negative charge from the carbonic of sodium alginate. As shown, the zeta potential shift of ALG-Zn-Mt was much more significant than ALG-Na-Mt indicating that the ionic interaction between Zn-Mt and sodium alginate was much stronger than Na-Mt due to its positive charge, and the  $\text{Zn}^{2+}$  (divalent metal ion) induction effect on ALG crosslinking which was reported by previous research [25]. After loading triazolone, a positive shift happened for both ALG-Na-Mt and ALG-Zn-Mt due to the interaction between double-bond from triazolone and negative electrons from the carrier. While under acid conditions, the value of negative zeta potential became much smaller due to the positive charge of hydrogen ion in solution. Hydrogen ion also exchange with zinc ion in carrier leading to the decrease in Zn-Mt zeta potential. On the other hand, the interaction between hydroxide ion and zinc ion or sodium ion weakened the interaction of Mt with ALG or triazolone under basic conditions. As a result, the value of zeta potential of the samples became very small while modified with ALG and loading drug.

As shown by XPS analysis in Fig. 5, the binding energy (BE) of O 1s (Fig. 5a) increased from 531.47 eV to 542.5 eV after ALG encapsulation due to the electronic interaction between carrier and ALG indicated by their Zeta potential characterization. And the BE of Tri/ALG-Zn-Mt increased up to 531.72 eV. A similar trend can be observed in the XPS spectrum of Si 2p in Fig. 5b. The BE of Zn 2p<sub>3/2</sub> (Fig. 5c) increased from 1021.43 eV to 1021.52 eV after encapsulated by ALG due to alginate crosslinking induced by zinc ion in accordance with SEM images shown in Fig. 4. Further, the BE of zinc ion belonged to Tri/ALG-Zn-Mt increased from 1021.52 eV to 1021.72 eV after loading triazolone due to the electronic interaction between the carrier and triazolone in accordance with the zeta potential results. Meanwhile, the BE of carbon kept constant

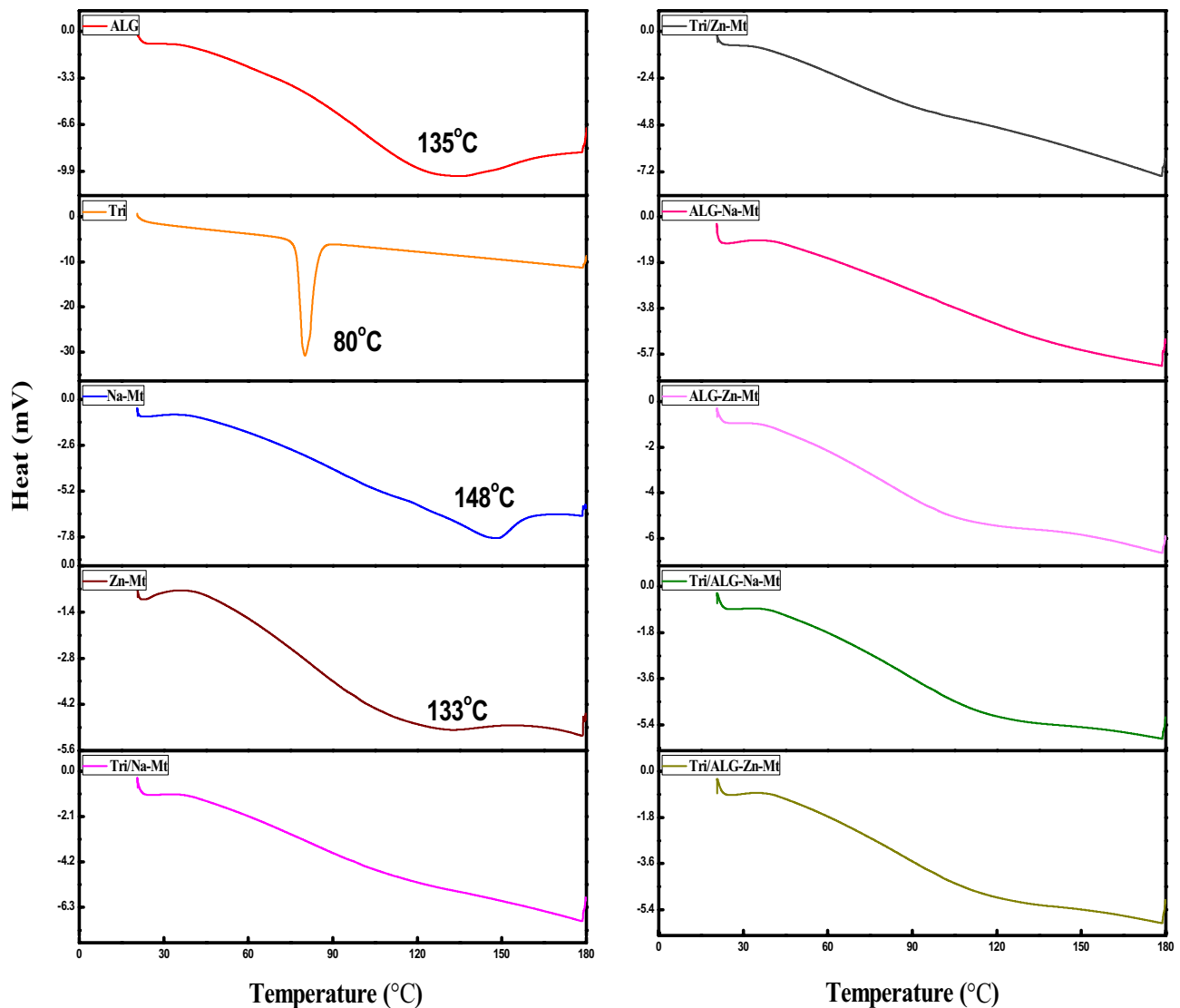


**Fig. 3** DSC thermograms of the samples

(Fig. 5d) indicating the weak interaction among CTAB, ALG and triazolone.

The  $N_2$  adsorption/desorption isotherms of Na-Mt, Zn-Mt, ALG-Na-Mt, and ALG-Zn-Mt (Fig. 6) belonged to type III (the slope of the curves was increasing) with H3 hysteresis loop which convinced the layer structures and selective adsorption capacity of the samples. What's more, ALG encapsulation would significantly decrease its BET surface and pores volume due to pores blocked by ALG especially for ALG-Na-Mt which decreased from  $65.89 \text{ m}^2/\text{g}$  to  $20.31 \text{ m}^2/\text{g}$  calculated by BJH method from desorption isotherms (Table 2). Meanwhile, the modification draw slight effect on the pore size in accordance with the XRD results mentioned above. Zinc ion acted as calcium ion to induce ALG crosslinking. The strong ionic interaction between the zinc ion and ALG prevented

the agglomeration of ALG in the pores of Mt. As a result, ALG-Zn-Mt has the highest adsorption capacity up to  $17.75 \text{ mg/g}$  with much larger BET surface area than ALG-Na-Mt. On the contrary, the adsorption capacity of ALG-Na-Mt was lowest ( $10.75 \text{ mg/g}$ ) due to the pore blocked by ALG agglomeration.

### 3.2 Sustained release performance

The sustained release curves of Tri/Zn-Mt at various pH (Fig. 7a) was in a release speed sequence of  $\text{pH } 5 > \text{pH } 7 \approx \text{pH } 9$ . And the accumulated release percentages in 200 h were 65.9%, 53.7%, and 51.1% at pH 5, pH 7, and pH 9, respectively. The difference of the points in sustained release curves was all in the range of error bar after 150 min indicating that the accumulated release

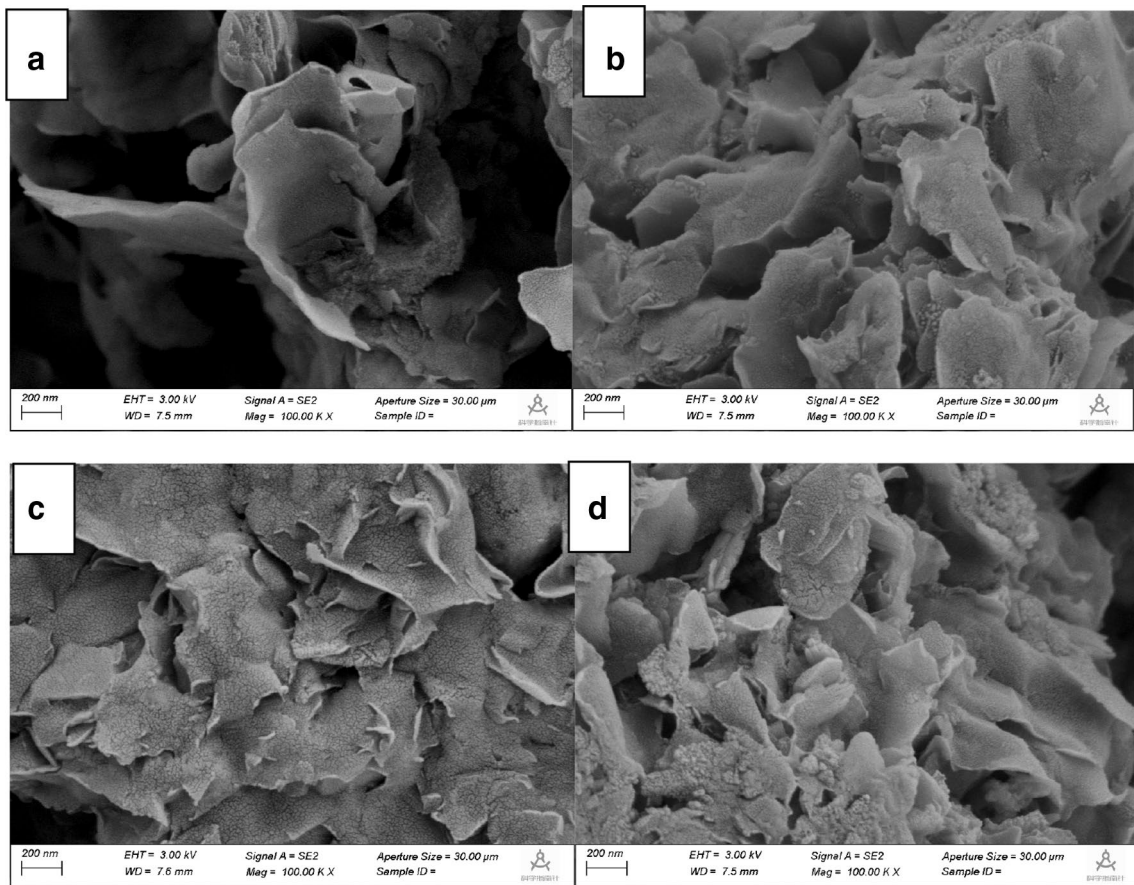


**Fig. 4** SEM image of Na-Mt (a), Zn-Mt (b), ALG-Na-Mt (c), and ALG-Zn-Mt (d)

**Table 1** The Zeta potential of Na-Mt, Zn-Mt, ALG-Na-Mt, ALG-Zn-Mt, Tri/ ALG-Na-Mt, Tri/ ALG-Zn-Mt under different pH conditions

Samples	pH=5	pH=7	pH=10
Na-Mt	-3.74 ± 1.65	-24.66 ± 0.32	-22.49 ± 2.80
Zn-Mt	8.49 ± 1.41	16.29 ± 0.67	-17.56 ± 3.77
ALG-Na-Mt	-7.30 ± 5.74	-28.98 ± 0.43	0.04 ± 0.45
ALG-Zn-Mt	-8.13 ± 0.22	-19.65 ± 1.49	0.31 ± 0.34
Tri/ALG-Na-Mt	-5.50 ± 0.67	-8.72 ± 1.73	0.30 ± 0.22
Tri/ALG-Zn-Mt	-2.50 ± 1.15	-1.55 ± 0.74	0.00 ± 0.33

percentage of the samples didn't increase after attained the adsorption-disorption balance. Under acid conditions, the zinc ion in Mt exchanged with hydrogen ion in the aqueous and the coordination bond between Zn<sup>2+</sup> and triazolone was broken down. The interaction between triazolone and substrate was weakened in consequence, and the drug release speed was accelerated. Meanwhile, the release speed sequence of Tri/ALG-Zn-Mt under various pH conditions (Fig. 7b) was pH 9 > pH 7 > pH 5 in according to the stability of ALG. Under basic conditions, the coordination between hydroxide ion and zinc ion apparently

weakened the interaction between zinc ion and ALG in consistent with the results from previous work [9]. Therefore, the release speed of Tri/ALG-Zn-Mt under basic conditions was faster than under acid or natural conditions. While under acid conditions, the release speed of Tri/ALG-Zn-Mt was smaller than under natural conditions because ALG was stable under acid conditions. The accumulated release percentages of Tri/ALG-Zn-Mt in 200 h were 45.8%, 64.9%, and 85.2% at pH 5, pH 7, and pH 9, respectively. The results indicated that Tri/ALG-Zn-Mt was pH sensitive and performed various sustained release behaviors with different pH value.

### 3.3 Sustained release kinetics

The sustained release curves of triazolone from Tri/Zn-Mt and Tri/ALG-Zn-Mt with various pH values were fitted to zero-order model, first-order model [26], Korsmeyer-Pappas [27], and Hixson-Crowell model [28], respectively (Table 3). In these equations, Mt was the accumulated release percentage at time t while M<sub>∞</sub> was the maximum release percentage of the samples. The drug release behavior of sustained release Tri/Zn-Mt

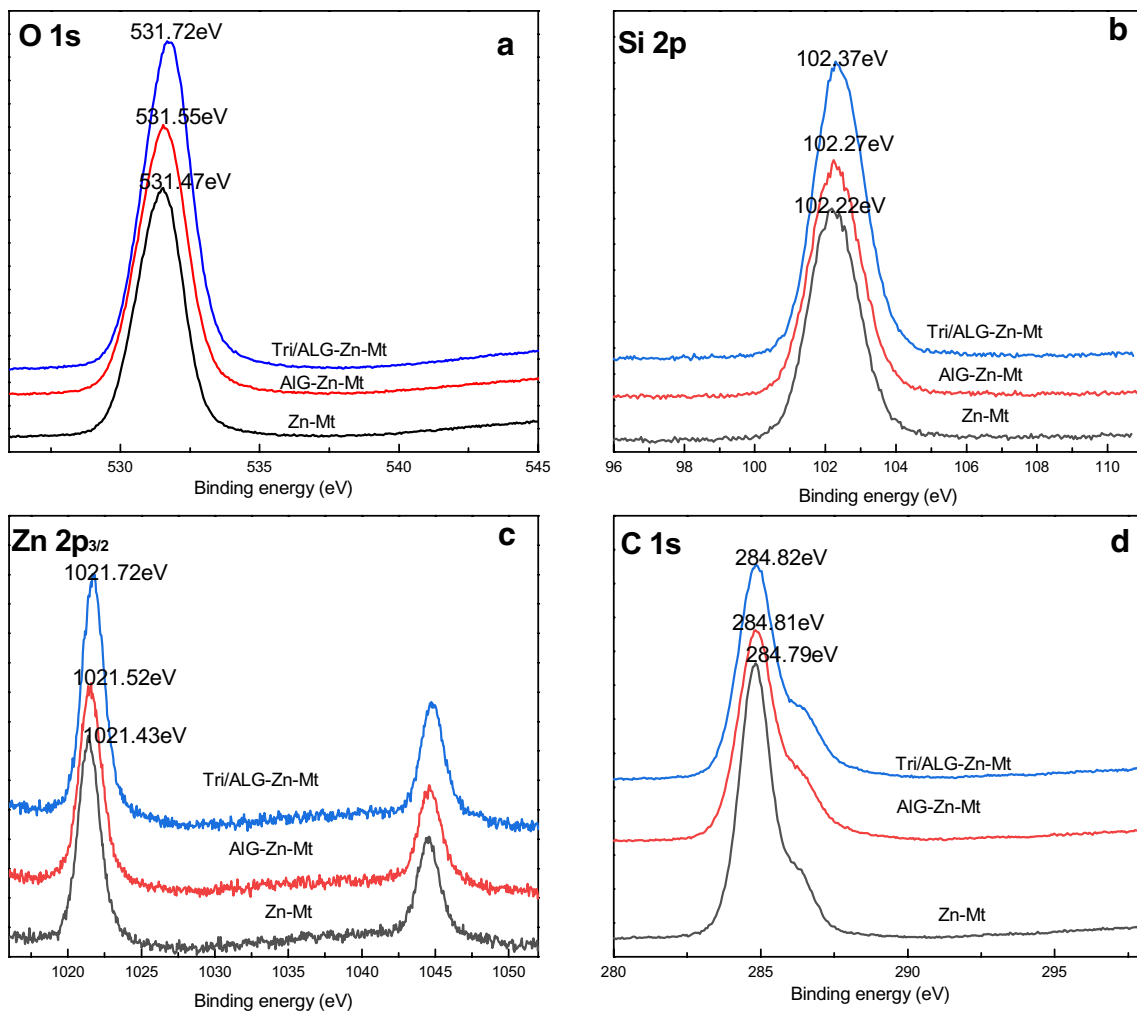


Fig. 5 O 1 s (a), Si 2p (b), Zn 2p<sub>3/2</sub> (c), and C 1 s (d) XPS spectra of Zn-Mt, ALG-Zn-Mt, and Tri/ALG-Zn-Mt

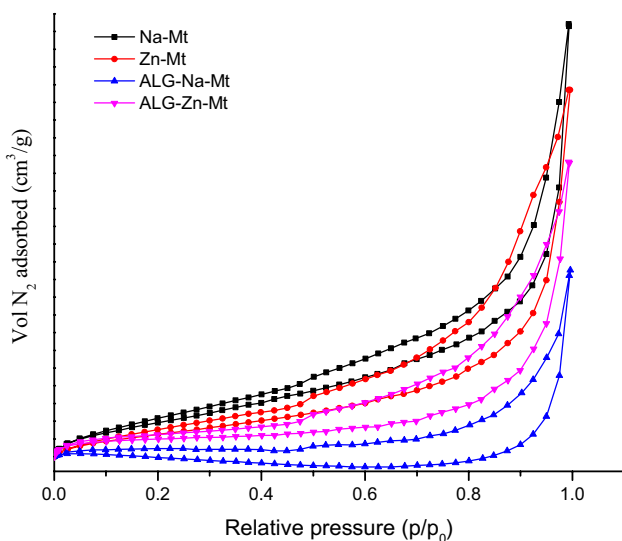
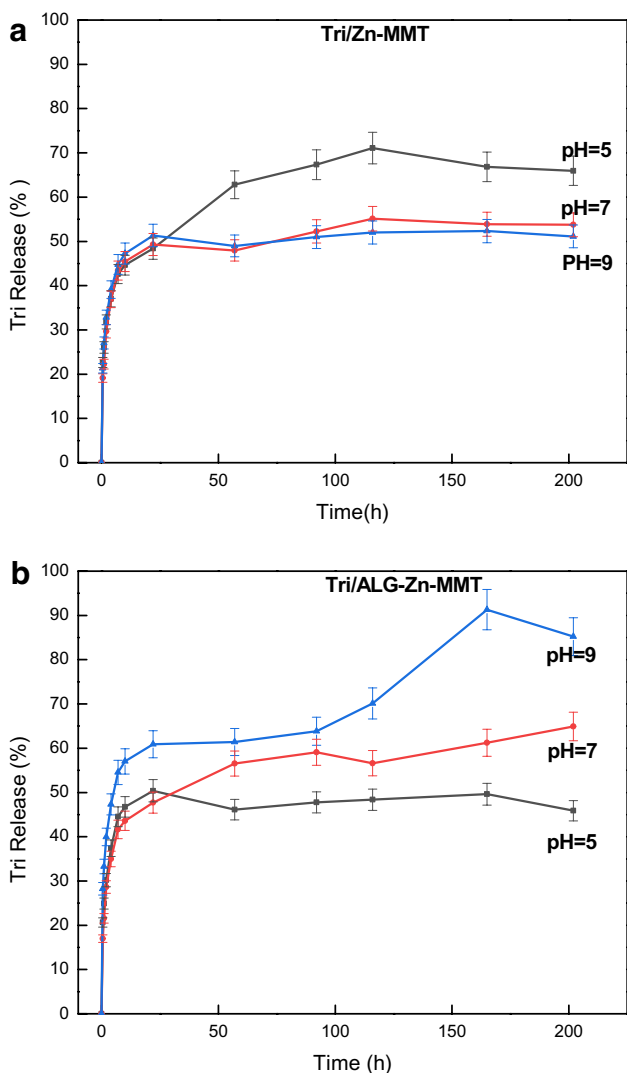


Fig. 6 N<sub>2</sub> adsorption/desorption isotherms (a) and pore size distribution (b) of Na-Mt, Zn-Mt, ALG-Na-Mt, and ALG-Zn-Mt

Table 2 The pore structural parameter and adsorption capacity (AC) of Na-Mt, Zn-Mt, ALG-Na-Mt, and ALG-Zn-Mt

Samples	BET surface(m <sup>2</sup> /g)	Pore volume (cm <sup>3</sup> /g)	Pore size(nm)	AC (mg/g)
Na-Mt	65.89	0.230	3.939	14.52
Zn-Mt	64.17	0.203	3.940	14.00
ALG-Na-Mt	20.31	0.107	3.936	10.75
ALG-Zn-Mt	47.64	0.164	3.935	17.75

particles was in consistent with the Korsmeyer–Pappas kinetic equation at pH 5. The diffusion coefficient  $n$  for time (t)  $n$  calculated from the kinetic equation was 0.1740 (< 0.45) indicating that the sustained release of triazolone from the particles was controlled by a Fickian diffusion mechanism [29–31]. Therefore,



**Fig. 7** Effect of pH values on sustained release performance of Tri/Zn-Mt (a) and Tri/ALG-Zn-Mt (b)

the difference of the concentration was the main impact on the release process. The drug release behavior was most consistent with the first-order kinetic at pH 7 and pH 9 and the release speed decreased convincing the synergic effect of drug diffusion and block effect from coordination bond on the release process. As depicted, the drug release behavior of Tri/ALG-Zn-Mt sustained release particles (Table 4) was in consistent with the Korsmeyer-Pappas kinetic equation at pH 7 and pH 9. The diffusion coefficient  $n$  was both below 0.45. When  $pH = 5$ , the sustained release curve fitted with first-order most caused by the synergic effect of drug diffusion, and ALG block effect suggesting that the pH-sensitivity of

Tri/ALG-Zn-Mt was mainly controlled by the stability of ALG. In summary, the release behavior of Tri/ALG-Zn-Mt was depicted in consideration of kinetic mechanism and the characterization results in this work (Fig. 8). The zinc ion in the Mt also played a similar role as calcium ion to induce ALG crosslinking which prevented the agglomeration of ALG and made ALG highly dispersed in pores. The layer of ALG was the main barrier for triazolone delivery during the sustained release process of Tri/ALG-Zn-Mt under acid conditions. While under basic conditions, hydroxide ion would compete with ALG to interact with zinc ion. As a result, the ALG would be peeled off, and the released speed would be accelerated.

#### 4 Conclusions

In conclusion, zinc (II) montmorillonite encapsulated by ALG was prepared for triazolone delivery with pH-sensitivity. The SEM images indicated that the regular layer structure and pore volume were well-maintained for ALG-Zn-Mt after ALG encapsulation. Zinc ion played a similar role as calcium ion to induce ALG crosslinking which made ALG highly dispersed in the layer structure of the Mt. The characterization also confirmed the existence of the electrostatic interaction between ALG and Mt (especially for negative charged Zn-Mt) which formed a ropy network among the particles. The electronic interaction between zinc ion and triazolone detected by the zeta potential characterization strengthened the interaction between drug and carrier. Therefore, the BET surface of ALG-Zn-Mt was much higher than ALG-Na-Mt. Besides, ALG-Zn-Mt has the highest adsorption capacity up to 17.75 mg/g. On the other hand, the adsorption capacity of ALG-Na-Mt was lowest (10.75 mg/g) due to the pore blocked by ALG agglomeration. Tri/ALG-Zn-Mt also showed significant pH-sensitivity after loading triazolone due to the different stability of ALG under different pH conditions. And triazolone released fastest from Tri/ALG-Zn-Mt at  $pH = 9$  caused by the broken of ionic balance inside leading to the sodium alginate peeled off from the particles. The sustained release curves of Tri/ALG-Zn-Mt were in consistent with the Korsmeyer-Pappas kinetic equation controlled by a Fickian diffusion mechanism under basic and neutral conditions. While the sustained release curve fitted with first-order equation under acid conditions due to the synergic effect of drug diffusion and ALG block effect on the drug release process.



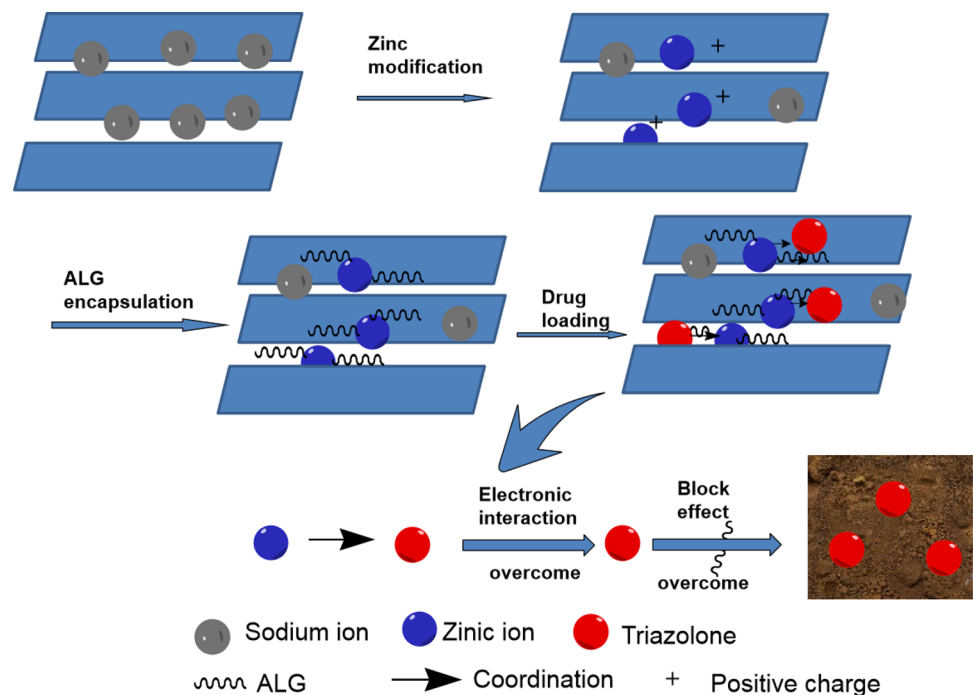
**Table 3** Fitting results for release curves of Zn–Mt in various pH values

Kinetic model	Fitting equation	R <sup>2</sup>
Zero-order	$\frac{M_t}{M_\infty} = \begin{cases} 37.4762 + 0.2024x, \text{PH} = 5 \\ 35.3114 + 0.1258x, \text{PH} = 7 \\ 37.8578 + 0.0955x, \text{PH} = 9 \end{cases}$	0.6802
		0.5026
		0.3999
First-order	$\frac{M_t}{M_\infty} = \begin{cases} 60.5555(1 - \exp(-0.2594x)), \text{PH} = 5 \\ 50.2276(1 - \exp(-0.4645x)), \text{PH} = 7 \\ 49.2003(1 - \exp(-0.6787x)), \text{PH} = 9 \end{cases}$	0.7009
		0.8728
		0.8668
Korsmeyer–Peppas	$\frac{M_t}{M_\infty} = \begin{cases} 28.9127x^{0.1740}, \text{PH} = 5 \\ 28.7336x^{0.1325}, \text{PH} = 7 \\ 31.8689x^{0.1056}, \text{PH} = 9 \end{cases}$	0.9571
		0.8594
		0.7995
Hixson–Crowell	$\frac{M_t}{M_\infty} = \begin{cases} (3.3891 + 0.0044x)^3, \text{PH} = 5 \\ (3.3008 + 0.0031x)^3, \text{PH} = 7 \\ (3.3697 + 0.0028x)^3, \text{PH} = 9 \end{cases}$	0.6309
		0.4763
		0.3818

**Table 4** Fitting results for release curves of ALG–Zn–Mt in various pH values

Kinetic model	Fitting equation	R <sup>2</sup>
Zero-order	$\frac{M_t}{M_\infty} = \begin{cases} 36.5974 + 0.0787x, \text{PH} = 5 \\ 33.9812 + 0.1853x, \text{PH} = 7 \\ 44.3032 + 0.2380x, \text{PH} = 9 \end{cases}$	0.2961
		0.6695
		0.7857
First-order	$\frac{M_t}{M_\infty} = \begin{cases} 46.8573(1 - \exp(-0.6520x)), \text{PH} = 5 \\ 55.9688(1 - \exp(-0.2791x)), \text{PH} = 7 \\ 68.2822(1 - \exp(-0.4492x)), \text{PH} = 9 \end{cases}$	0.8764
		0.8275
		0.6132
Korsmeyer–Peppas	$\frac{M_t}{M_\infty} = \begin{cases} 30.8700x^{0.0990}, \text{PH} = 5 \\ 26.3212x^{0.1738}, \text{PH} = 7 \\ 35.9422x^{0.1579}, \text{PH} = 9 \end{cases}$	0.7031
		0.9476
		0.9028
Hixson–Crowell	$\frac{M_t}{M_\infty} = \begin{cases} (3.3299 + 0.0020x)^3, \text{PH} = 5 \\ (3.2752 + 0.0043x)^3, \text{PH} = 7 \\ (3.5660 + 0.0048x)^3, \text{PH} = 9 \end{cases}$	0.2820
		0.6325
		0.7674

**Fig. 8** The schematic diagram of preparation and drug release of Tri/ALG-Zn-Mt



**Acknowledgements** This research was funded by Natural Science Foundation of Guangdong Province (Grant No. 2017A030311003), Science and Technology Program of Guangzhou, China (Grant No. 201707010473), Guangzhou Science and Technology Program key projects (Grant Nos. 201704020025, 201903010011).

### Compliance with ethical standards

**Conflict of interest** The authors declare that they have no conflict of interests.

### References

- Schmack R, Eckhardt B, Koch G, Ortel E, Kraehnert R (2016) ZnO coatings with controlled pore size, crystallinity and electrical conductivity. *Mater Sci* 22:74–81
- Kang W, Huang G, Geng Q, Hou W, Yao Y, Xu B, Xing B, Zhang C (2018) Effect of de-ashing strategies on pore structure and electrochemical performance of activated carbons for supercapacitors. *Mater Sci* 24:247–252
- Sanusi OM, Benelfellah A, Hocine NA (2020) Clays and carbon nanotubes as hybrid nanofillers in thermoplastic-based nanocomposites—a review. *Appl Clay Sci* 185:105408
- Kumar S, Bhanjana G, Sharma A, Sidhu MC, Dilbaghi N (2014) Synthesis, characterization and on field evaluation of pesticide loaded sodium alginate nanoparticles. *Carbohydr Polym* 101:1061–1067
- Jain S, Datta M (2016) Montmorillonite-alginate microspheres as a delivery vehicle for oral extended release of venlafaxine hydrochloride. *J Drug Deliv Sci Tec* 33:149–156
- Suarez-Gonzalez D, Barnhart K, Saito E, Vanderby R, Hollister SJ, Murphy WL (2010) Controlled nucleation of hydroxyapatite on alginate scaffolds for stem cell-based bone tissue engineering. *J Biomed Mater Res A* 95:222–234
- Liang Y, Liu C, Liao S, Lin Y, Tang H, Liu S, Lai I, Wu K (2012) Cosynthesis of cargo-loaded hydroxyapatite/alginate core-shell nanoparticles (HAP@Alg) as pH-responsive nanovehicles by a pre-gel method. *ACS Appl Mater Inter* 4:6720–6727
- Bastakoti BP, Sukegawa H, Wu KCW, Yamauchi Y (2014) Synthesis of porous iron oxide microspheres by a double hydrophilic block copolymer. *RSC Adv* 4:9986–9989
- Chen HY, Lin YS, Zhou HZ, Zhou XH, Gong S, Xu H (2016a) Highly efficient alginate sodium encapsulated chlorpyrifos/copper(II) Schiff base mesoporous silica sustained release system with pH and ion response for pesticide delivery. *RSC Adv* 6:114714–114721
- Yuan W, Dong H, Li CM, Cui X, Yu L, Lu Z, Zhou Q (2007) pH-Controlled construction of chitosan/alginate multilayer film: characterization and application for antibody immobilization. *Langmuir* 23:13046–13052
- Chen H, Lin Y, Zhou H, Zhou X, Gong S, Xu H (2016b) Synthesis and characterization of chlorpyrifos/copper (II) Schiff base mesoporous silica with pH-sensitivity for pesticide sustained release. *J Agr Food Chem* 64:8095–8102
- Lin S, Zhou T, Yin S (2017) Properties of thermally treated granular montmorillonite-palygorskite adsorbent (GMPA) and use to remove  $Pb^{2+}$  and  $Cu^{2+}$  from aqueous solutions. *Clay Clay Miner* 65:184–192
- Mishra AK, Allauddin S, Narayan R, Aminabhavi TM, Raju KVS (2012) Characterization of surface-modified montmorillonite nanocomposites. *Ceram Int* 38:929–934
- Yang Y, Zhu R, Chen Q, Fu H, He Q, Zhu J, He H (2020) A novel multifunctional adsorbent synthesized by modifying acidified organo-montmorillonite with iron hydroxides. *Appl Clay Sci* 185:105420
- Hu XL, Huang YP, Zhang AQ, Zhao XR (2014) Adsorption of organic pollutants by ferric oxide modified montmorillonite. *Adv Mater Res* 955–959:80–83

16. Radian A, Fichman M, Mishael Y (2015) Modeling binding of organic pollutants to a clay–polycation adsorbent using quantitative structural–activity relationships. *Appl Clay Sci* 116–117:241–247
17. Iliescu RI, Andronescu E, Ghitulica CD, Voicu G, Ficai A, Hoteteu M (2014) Montmorillonite–alginate nanocomposite as a drug delivery system–incorporation and in vitro release of irinotecan. *Int J Pharmaceut* 463:184–192
18. Hassani A, Soltani RDC, Karaca S, Khataee A (2015) Preparation of montmorillonite–alginate nanobiocomposite for adsorption of a textile dye in aqueous phase: Isotherm, kinetic and experimental design approaches. *J Ind Eng Chem* 21:1197–1207
19. Kpannieu DE, Ruby C, Coulibaly L, Abdelmoula M, Mallet M (2018) Removal of phosphate by Ivory coast shale in a homogeneous reactor and under hydrodynamic conditions: influence of soluble species. *Clay Clay Miner* 66:500–514
20. Kresge CT, Leonowicz ME, Roth WJ, Vartuli JC, Beck JS (1992) Ordered mesoporous molecular sieves synthesized by a liquid-crystal template mechanism. *Nature* 359:710–712
21. Song Y, Zeng HH, Liang YP (2014) Progress on organochlorine pesticides (OCPs) in China's lakes. *Adv Mater Res* 1010–1012:467–471
22. Wang P, Yin Y, Guo Y, Wang C (2016) Preponderant adsorption for chlorpyrifos over atrazine by wheat straw-derived biochar: experimental and theoretical studies. *RSC Adv* 6:10615–10624
23. Gerstl Z, Nasser A, Mingelgrin U (1998) Controlled release of pesticides into water from clay–polymer formulations. *J Agr Food Chem* 46:4245–4253
24. Tao Y et al (2015) A quick, easy, cheap, effective, rugged, and safe method for the simultaneous detection of four triazolone herbicides in cereals combined with ultrahigh performance liquid chromatography with tandem mass spectrometry. *J Sep Sci* 37:2340–2348
25. Şanlı O, Işıkhan N (2006) Controlled release formulations of carbaryl based on copper alginate, barium alginate, and alginic acid beads. *J Appl Polym Sci* 102:4245–4253
26. Mohsin A, Sun J, Khan IM, Hang H, Tariq M, Tian X, Ahmeda W, Niazi S, Zhuang Y, Chu J, Mohsin MZ, Rehman S, Mohsin MZ (2019) Sustainable biosynthesis of curdlan from orange waste by using *alcaligenes faecalis*: a systematically modeled approach. *Carbohydr Polym* 205:626–635
27. Korsmeyer RW, Gurny R, Doelker E, Buri P, Peppas NA (1983) Mechanisms of solute release from porous hydrophilic polymers. *Int J Pharmaceut* 15:25–35
28. Costa P (2001) An alternative method to the evaluation of similarity factor in dissolution testing. *Int J Pharmaceut* 220:77–83
29. Voogt JA, Hirte A, Meinders MB (2011) Predictive model to describe water migration in cellular solid foods during storage. *J Sci Food Agr* 91:2537–2543
30. Giegloa W, Wormeesterb H, Wesslingc ME, Benes N (2013) Temperature-induced transition of the diffusion mechanism of n-hexane in ultra-thin polystyrene films, resolved by in-situ spectroscopic ellipsometry. *Polymer* 54:341–348
31. Lagorce-Tachon A, Karbowiak T, Simon JM, Gougeon R, Bellat JP (2014) Diffusion of oxygen through cork stopper: is it a Knudsen or a Fickian mechanism? *J Agr Food Chem* 62:9180–9185

**Publisher's Note** Springer Nature remains neutral with regard to jurisdictional claims in published maps and institutional affiliations.